IMAGE PROCESSING SYSTEM TO ANALYZE DROPLET DISTRIBUTIONS IN SPRAYS

Gary P. Bertollini

Larry M. Oberdier

Yong H. Lee

Instrumentation Department

General Motors Research Laboratories

Warren, Michigan 48090-9057

December 7, 1984

ABSTRACT

The General Motors Research Laboratories has developed an image processing system which automatically analyzes the size distributions in fuel spray video images. Images are generated by using pulsed laser light to freeze droplet motion in the spray sample volume under study. This coherent illumination source produces images which contain droplet diffraction patterns representing the droplets degree of focus. Thousands of images are recorded per sample volume to get an ensemble average of the distribution at that spray location. After image acquisition the recorded video frames are replayed and analyzed under computer control.

The analysis is performed by extracting feature data describing droplet diffraction patterns in the images. This allows the system to select droplets from image anomalies and measure only those droplets considered in focus. The system was designed to analyze sprays from a variety of environments. Currently these are an ambient spray chamber, a high pressure high temperature spray facility, and sprays in a running engine.

Unique features of the system are the totally automated analysis and droplet feature measurement from the grayscale image. Also it can distinguish non-spherical anomalies from droplets which allows sizing of droplets near the spray nozzle.

This paper describes the feature extraction and image restoration algorithms used in the system. Preliminary performance data is also given for two experiments. One experiment gives a comparison between a synthesized distribution measured manually and automatically. The second experiment compares a real spray distribution measured using current methods against the automatic system.

KEYWORDS

particle sizing and spray analysis; droplet sizing; spray characterization; image processing;

INTRODUCTION

Basic research is being conducted to relate the combustion process and the design and placement of fuel injectors. This is being accomplished by studying fuel spray droplet dynamics. The fuel spray study utilizes a system which records video images of spray droplets directly from a variety of fuel spray environments. These include an ambient spray chamber[1,2], a high temperature, high pressure test chamber, and the combustion chamber of a running engine[3].

Because of the harsh spray environments the analysis of video images at General Motors Research Laboratories is currently done manually by observing the images on a TV and

selecting only "in focus" droplets for velocity and size measurements. Manual data reduction is time consuming, tedious and inconsistent for different operators. These problems led to the development of an automatic system for droplet measurement. This system should access archived image data and extract droplet size information without manual intervention. The system must also analyze poor quality images containing low frequency intensity gradients which exceed droplet contrast levels. The realization of these requirements has pushed the capabilities of this spray analysis system beyond any other direct imaging system[4,5,6,7,8].

HARDWARE

Figure 1 shows a block diagram of the hardware utilized in this study. For further details, refer to Oberdier paper[9]. Images are created by direct imaging of a spray sample area on a high resolution CCD (charge coupled device) array camera . This camera has a sensor resolution of 380 X 480 picture elements (pixels). Illumination of the sample volume is provided by a pulsed 100 μJ nitrogen laser at a wavelength of 337 nm. The 10 ns laser pulses are collimated and passed through the test volume perpendicular to the spray. The imaging lense used has a 117 mm focal length. The recording camera is positioned to give a resolution of 3.3 um per image pixel. This magnification allows a 1.2 X

1.5 mm field of view at the focal plane. Because of the filter operation performed by the software to remove low frequency image degradation, the measurable droplet diameter range is limited at 5 to 50 pixels. This translates an effective droplet diameter range of 16 to 165 um. Thus the imaging lense is switched to accommodate other ranges.

Image acquisition is accomplished by using a microcomputer based controller which synchronizes laser firing, camera scanning and image storage to the experimental process. The controller was developed at General Motors and will synchronize image acquisition at a particular engine crank angle or free run at standard video rates (30 frames per second). Images are stored on a magnetic video disk recorder which allows full frame, random access of the images. After the data is collected the stored images are digitized and analyzed automatically by a Vicom image analysis system. This system digitizes each image to a 512 X 512 pixel array at 8 bits of resolution per pixel. It should be noted that current camera and recorder technologies limit the realization of this specification to 6 bits of of intensity resolution and the horizontal bandwidth to 450 lines.

IMAGE PROCESSING ALGORITHMS

Image processing algorithms were applied to perform the following steps.

1. Image normalization - Remove low frequency degradation in the recorded images.
2. Segmentation - Find places in the image which may be the centroid of droplets.
3. Feature extraction - Extract feature data from the image restored in step one at those centroid locations.
4. Classification - Decide if the object is an in focus droplet by using extracted diffraction feature data.

Image Restoration

The fuel spray images recorded from the high temperature, high presure chamber and the running engine chamber have low frequency intensity degradation. This is caused by droplets which hit the observation window, refracting gradients in the optical path, and sensor scan variations. This degradation has intensity values which can be similar to droplet intensities. This degradation is removed in the following manner.

As discussed in[10,11,12], an image formation model can be represented mathematically as:

(1) $g(x,y) = d(x,y)f(x,y) + n(x,y) + b$

where

$g(x,y)$ = detected image

$f(x,y)$ = original image

$d(x,y)$ = multiplicative noise

$n(x,y)$ = additive noise

b = intensity bias.

We assume that the low frequency degrading function is represented by $d(x,y)$. The additive noise $n(x,y)$ represents high frequency (pixel to pixel) digitization and camera sensor noise. The b term is added to the model by the authors to account for any intensity bias which may be added to the image by video circuitry or ambient light.

Solving for the original image, $f(x,y)$, before the degradation occurred results in:

(2) $f(x,y) = [g(x,y) - n(x,y) - b] / d(x,y)$.

Instead of estimating the additive noise and subtracting it from the image $g(x,y)$, the image $g(x,y)$ is passed through a low pass filter. This is accomplished by convolving $g(x,y)$ with a Gaussian impulse response whose coefficients are given as

0.0	.0004	.002	.0004	0.0
.0004	.032	.113	.032	.0004
.002	.113	.4013	.113	.002
.0004	.032	.113	.032	.0004
0.0	.0004	.002	.0004	0.0

Figure 2 shows a plot of g(x,y) before and after the Gaussian operation. The intensity bias, b is calculated as being the lowest intensity value in the image after the additive noise is removed. This bias is subtracted from every image point in the image.

The last step in this image normalization process is the removal of the low frequency degradation, d(x,y). This is first estimated by using a nonlinear filtering technique called morphological filtering. This was selected over other low pass filters because it preserves edge structure. The effect of this filter operation is to delete image objects smaller than the defined size of the filter. This leaves an image which contains only the background intensity levels. Therefore to estimate d(x,y), the filter size is selected to be larger than the largest object to be measured.

A simple representation of this filter as given in[13] is:

(3) $d(s,t) = \max [\, f(x,y) \,.\, \mathrm{circ}\, [\sqrt{(x-s)^2+(y-t)^2}\ /r_o]]$

where $d(s,t)$ = resulting image

$f(x,y)$ = original image

$\mathrm{circ}\, [\sqrt{(x-s)^2+(y-t)^2}\ /r_o]$ describes the circular structuring element with radius r_o and equals:

1 for $\sqrt{(x-s)^2+(y-t)^2}\ /r_o \ <= \ 1$

0 otherwise

The max function propagates local image intensity maxima over the filter size defined by r_o for every pixel in the image. The original boundaries are preserved by performing a reverse propagation on the transformed image:

(4) $d(s,t) = \min[\ f(x,y) \,.\, \mathrm{circ}\, [\sqrt{(x-s)^2+(y-t)^2}\ /r_o]]$

The min function propagates local image intensity minima over the filter size defined by r_o for every pixel in the image. To normalize the image, the estimated $d(x,y)$ is divided into the intermediate image, $(g(x,y) - n(x,y) - b)$ per equation (2).

Figure 3, 4 and 5 show an original image, its background estimate, d(x,y) using this filter, and the normalized image after division.

SEGMENTATION - Locating candidate objects

By utilizing the previous image restoration algorithm, intensity thresholding can be used to segment areas which may or may not be droplets, i.e., candidates[14]. Image threshold levels are selected by analyzing the intensity histogram[15,16]. It is assumed that the largest distribution in the histogram corresponds to the background intensity. The midpoint of this distribution's positive slope is selected as the threshold level if the histogram is unimodal. If there is a peak prior to the background peak the valley between both distributions is selected.

The output of the threshold operation is a binary image in which the dark areas correspond to candidates. Region boundaries are generated by using a 4 adjacency border algorithm[17]. This algorithm allows a fast way to generate all object boundaries at one time by treating the image as a whole. It is defined mathematically as

$$(5)\quad B(x,y) = S(x,y) * [\, \bar{S}(x-1,y) + \bar{S}(x+1,y) + \bar{S}(x,y+1) + \bar{S}(x,y-1) \,]$$

where

$B(x,y)$ = boundary image

$S(x,y)$ = original threshold image

$\bar{S}(x,y)$ = logical negation of $S(x,y)$

$*$ = logical AND

$+$ = logical OR.

The output of this algorithm is object edge pixels which define the object's boundary. Figures 6 and 7 show a threshold and its associated boundary image.

The image is scanned by a tracking algorithm which follows object boundaries and calculates the centroid, radius (a circle is fit to the points) and number that represents how good the boundary fits the circle. The centroids are points in the normalized image g(x,y) which will be used as feature extraction locations.

Feature Extraction

To extract features from candidate objects two curves are determined. Both curves are calculated by assuming symmetry around the centroids determined in the previous section. One curve is a radial intensity profile, the other a radial standard deviation. To accomplish this, the vector distance from each candidate's centroid to all neighboring points is

calculated. Neighboring points are averaged for an area spanning twice the radius value found when calculating the boundary centroid. The distance to neighboring points is modified to compensate for the aspect ratio induced by the camera. This is calculated using 0.8 times the vertical displacement. Intensity values for similar distance vectors are accumulated to get average radial intensity and radial standard deviation. See Figure 8.

Because of the way the centroid was selected two things are possible. First, the calculated intensity and deviation curves may or may not represent a droplet. Many kinds of anomalies are possible. For example the object could represent a multiple droplet cluster, a blob that was created by the selected threshold level or an anomaly created by edge effects after creating an image mosaic. Examples of these are shown in Figure 7. These anomalies are distinguished using the circular fit number generated during boundary tracking along with the intensity and deviation curves during the classification process. Secondly, the centroid may indicate a valid droplet but may not be the real object center. To correct this, the software attempts to reposition all droplet centers by using radial deviation information as an indication of best center position. Repositioning is done by calculating the standard deviation for the four quadrants of a candidate. See Figure 9. The derivative of the quadrant curves 2,3,4 is

cross correlated with the derivative of quadrant 1. The resulting correlation peaks are at index points which weight the direction of center repositioning in the following way:

(6) Delta X = TRUNCATE(0.5 + cosϕ (-Q2 - Q3 + Q4)) (7)

Delta Y = TRUNCATE(0.5 + sinϕ (Q2 - Q3 - Q4))

where ϕ = 45 degrees =(.707)

Q1-4 = correlation index values

This procedure iterates up to 5 times per candidate before aborting if the delta valves do not converge to zero. Assuming that the radial intensity profile corresponds to the diffraction pattern of a real droplet, a variety of features describing the pattern are calculated. Some of these features are :

1. Intensity profile slope at the droplet center.
2. Number of rings within the droplet.
3. Slope of intensity profile at droplet edge.
4. Droplet contrast.
5. Intensity profile overshoot height and width.
6. Droplet radius measured at the maximum profile slope at the droplet's edge.

Extracted features and where the feature is measured is shown on the curves in Figure 10. This figure was generated using theoretical radial intensity plots of an ideal opaque

100 micron sphere at 200 and 400 microns from the plane of focus.

A rudimentary classification procedure uses these and other features to select the radial intensity curves which represent droplets that are in the sample volume.

Experimental Procedure

Two preliminary experiments were run to quantify the accuracy of the automatic system vs. manual techniques. In the first, a slide of polystyrene microspheres was measured using a micrometer attached to a microscope (labeled MICROMETER in Figure 11). 500 measurements were made on the slide to get an ensemble average of the distribution. In a similar fashion 50 images at random slide positions were analyzed by the automatic system (VIDEO-AUTO). Images were acquired by illuminating the slide with a 5 mw helium neon laser. A CCD camera inline with the laser detected a sample area using the same 'experimental' optics described in the hardware section. The slide was held in a micropositioning device and images with a high droplet density were recorded. These same images were also measured manually on a video monitor using a scale (VIDEO-MANUAL).

In a second experiment, 400 images were recorded in the high pressure high temperature test facility using a Heptane gasoline spray. A nitrogen laser and vidicon camera was

used as the illumination source and sensor. The optics used were the same as in experiment 1. The images were manually measured on a video monitor by two different observers (VIDEO-MANUAL #1,#2) and also by the automatic system. Because this experiment measured a real spray the sample counts were corrected for depth of field effects. This procedure compensates for the fact that smaller droplets defocus faster than larger ones for equal distances from the imaging optics plane of focus. Therefor to account for a varying sample volume, the droplet size counts for the sample volume is multiplied by the ratio of depth of fields. The ratio is defined as the maximum measured size's depth of field divided by each size bin's depth of field. This increases count values for smaller droplet size bins exponentially.

A comparison of sizing the droplets manually vs. automatically is given for both experiments in Figures 11 and 12. Both figures compare the percentage of total count vs. droplet size. Also included is the linear, volume, and sauter mean diameters for each method.

Results

The first experiment is more controlled than the second because no decision is necessary on the observer's part as to whether or not a sphere (droplet) is in focus, and thus all objects were counted except for droplet clusters. In

experiment 1, the manual measurement using the video monitor varied from the measurement using the micrometer by a 2-6% range for the distribution's mean diameters. This includes errors induced in the measurement process (selecting the object boundaries in both cases is subjective) and actual distribution differences because of the small sample size (500 for the micrometer, 175 for the monitor) and human error.

The distribution's mean diameters calculated using the automatic system varied over a 3-9% range from the micrometer values. It measured 172 objects, 1 of which was an error.

In experiment 2, the manual #2 measurements varied 2-13% from manual #1 over the various mean diameters. Because this second experiment involved real spray images, a decision as to the selection of droplets by their degree of focus had to be made by the observers. 400 images were analyzed containing approximately 8000 candidate objects. The distribution size totalled 150 and 120 droplets for the #1 and #2 manual measurements respectively. Both manual measurements were averaged to provide mean diameter values to compare against the automatic system. The automatic system varied 5-16% from those average values. It selected 85 focused droplets.

The variation between measurements in both experiments is due to the small sample size and human measurement variations. size[18].

CLOSURE

A system has been developed which automatically measures droplet size distributions from video images. This offers a method to measure areas of spray distributions were conventional devices fail such as at the spray nozzle tip. This method may also be used to verify the calibration of other instruments. The accuracy of this technique has been evaluated by two preliminary experiments and was shown to be in the range of 2-16%. It is felt that this is very satisfactory range. From experience gained in these experiments we feel that a next step is a dual purpose experiment involving larger sample sizes. This would confirm our experimental results and at the same time characterize a spray.

ACKNOWLEDGMENTS

The authors gratefully acknowledge the following people at GMR for their assistance during the course of this project. Bruce Peters (FL) for discussions regarding spray diagnostics. Ather Quader (FL) for assistance in preliminary experiments on the CFR engine. Weston Meyer (MA) for the boundary curve fitting algorithm. Robert Lewis

(PH) and Richard Hall (PH) for consultation on and loan of optical equipment for droplet simulation. We also thank Julian Tishkoff, now with the Air Force Office of Scientific Research, for consultation and support during the beginning of this work.

REFERENCES

1. J. M. Tishkoff, Second International Conference on Liquid Atomization and Spray Systems, 10(1), (6),(1982).

2. J. M. Tishkoff, D. C. Hammond and A. R. Chraplyvy, J. Fluids Engineering, 104(9), 313 (1982).

3. B. D. Peters, "Laser-Video Imaging and Measurement of Fuel Droplets in a Spark-Ignition Engine," presented at the Conference on Combustion in Engineering, IME, (4),(1983).

4. C. Ramshaw, J. Inst. of Fuel, (7), 287 (1968).

5. C. S. Ow and R. I. Crane, Int. J. Heat and Flow, 2(1), 47 (1980).

6. M. C. Toner, M. J. Dix and H. Sawistowski, J Phys. E: Sci. Instrum. 11, 960 (1978).

7. C. S. Ow and R. I. Crane, J. Inst of Energy, (9), 119 (1981).

8. R. Fleeter, R. Toaz and V. Sarohia, ASME, reprint 82-WA/HT-23.

9. L. M. Oberdier, ASTM Symposium on Liquid Particle SIze Measurement Techniques, (6),123 (1983).

10. R. C. Dahlberg, Applications of Digital Image Processing III., SPIE, 207(8) ,(1979).

11. H. C. Andrews, Topics in Applied PhysicsPicture Processing and Digital Filtering, 6,1 (1979).

12. T. S. Huang, Topics in Applied physicsPicture Processing and Digital Filtering, 6,32 (1979).

13. E. Reinhardt, R. Erhardt, P. Schwarzmann, W. Bloss and R. Ott, The Intrn. Academy of Cytology Analytical and Quantitative Cytology, 1(2), 143 (1979).

14. K. S. Fu and J. K. Mui, Pattern Recognition, 13,3 (1980).

15. D. H. Ballard and C. M. Brown, "Computer Vision," 152-155 (1982).

16. T. Pavlidis, "Structured Pattern Recognition," 1, 65-69 (1977).

17. A. Rosenfield and A. C. Kak, "Digital Picture Processing," 333-352 (1976).

18. R. W. Tate, Proc. for the 2nd Intrn. Conf. on Liquid Atomization and Spray Systems, 12-4(6), (1982).

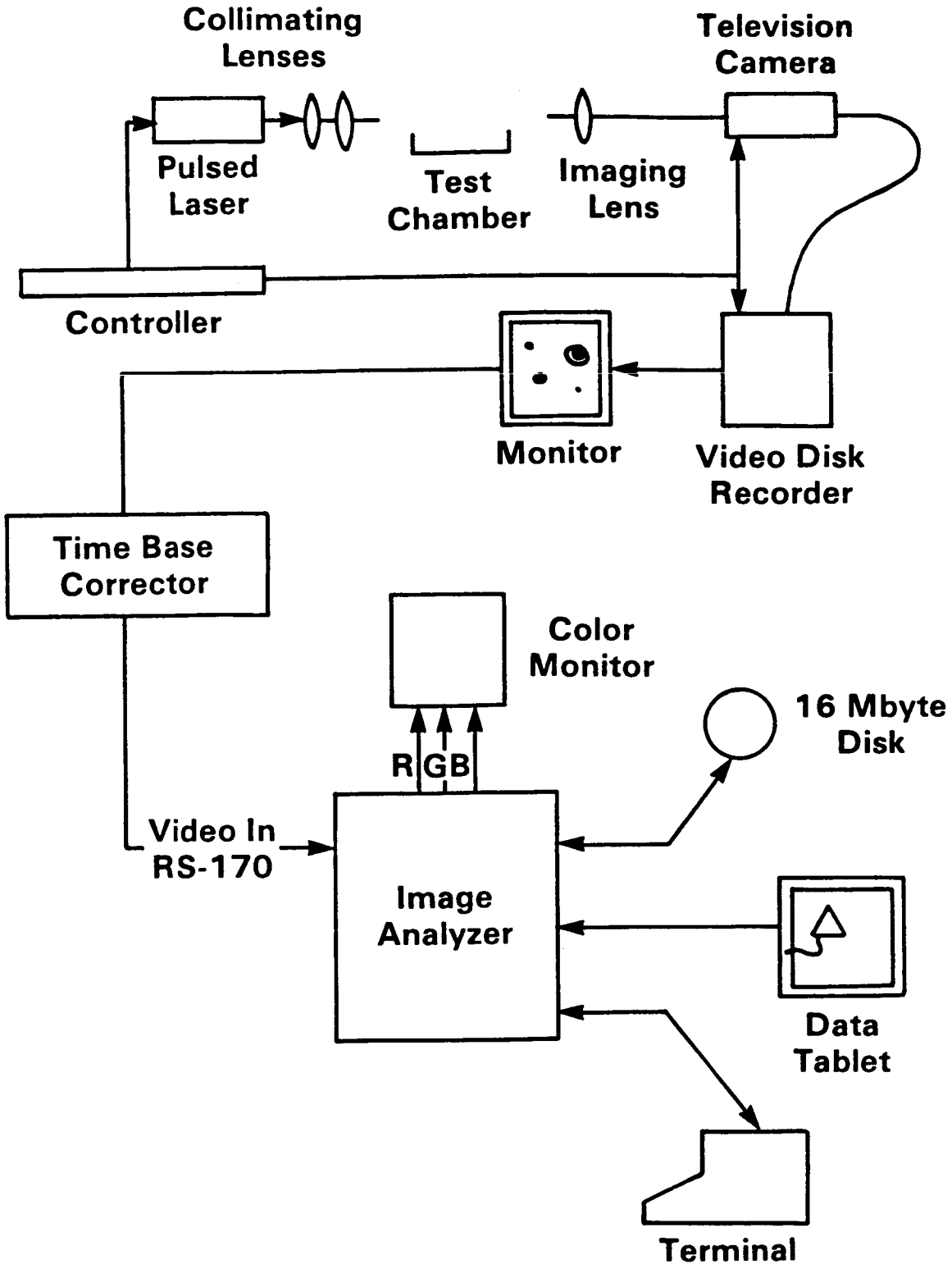

Figure 1. Equipment block diagram

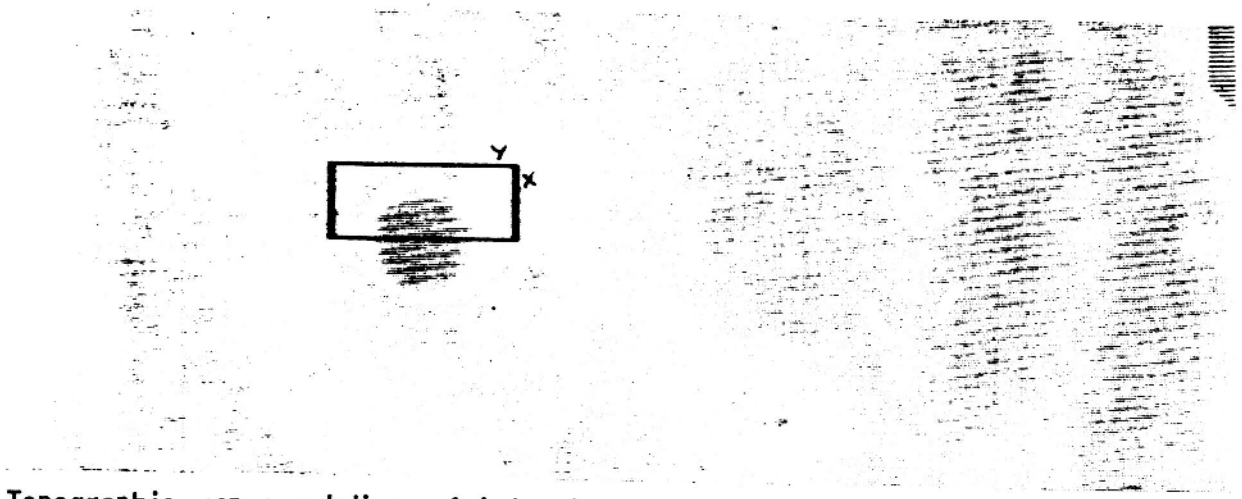

Topographic representation of intensity level in area marked above

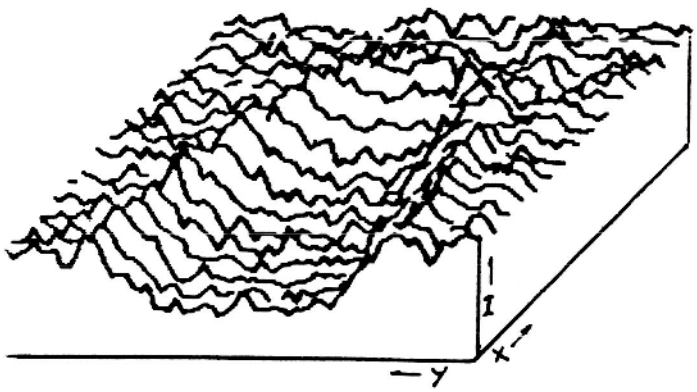

Original Image

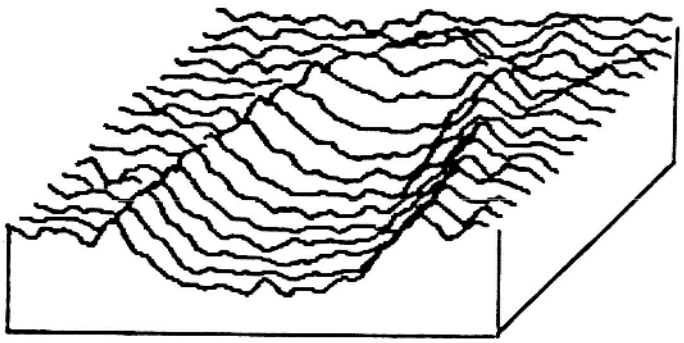

After Gausian Filter

Figure 2. Gaussian filtering operation

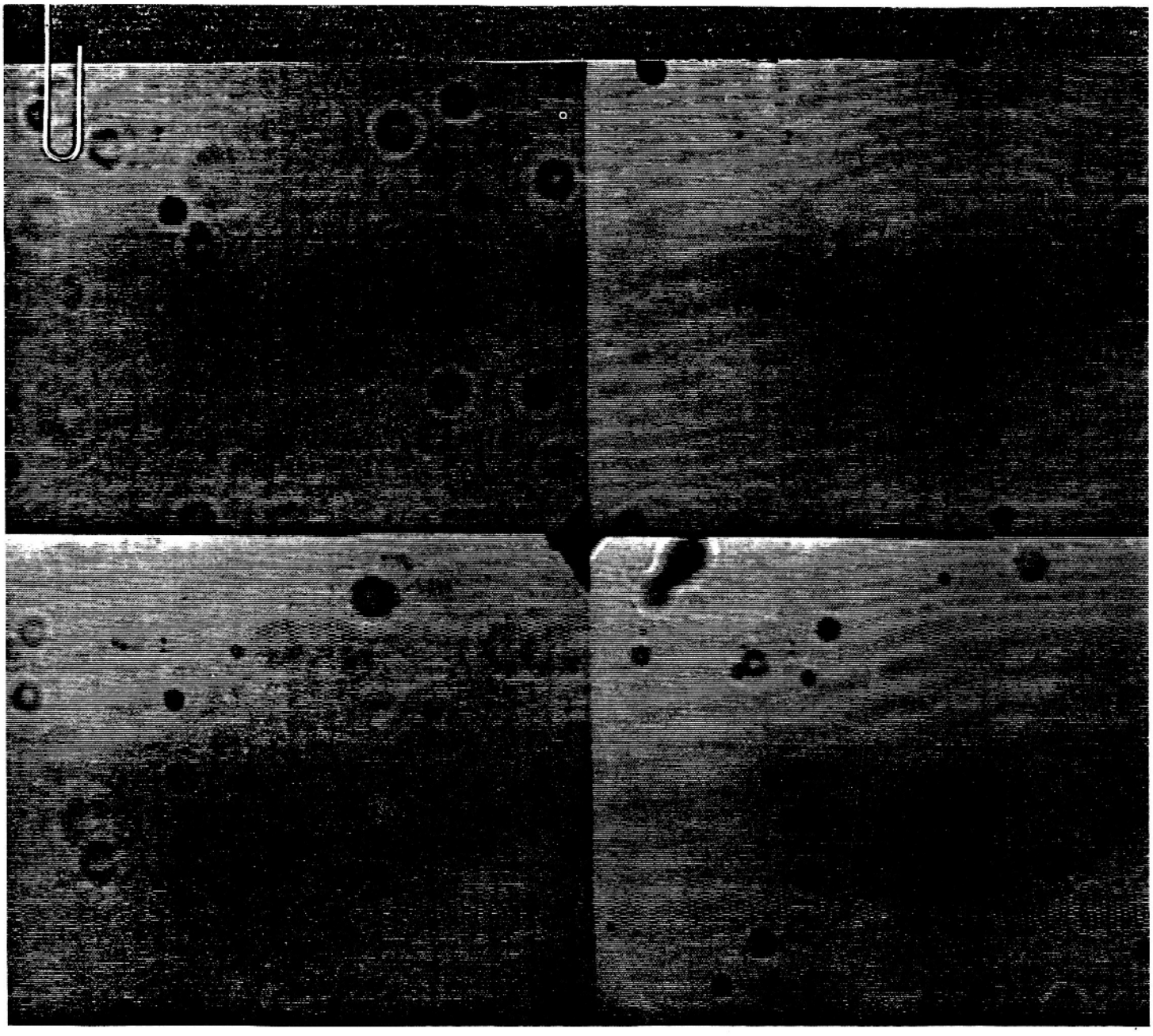

Figure 3. Original Image

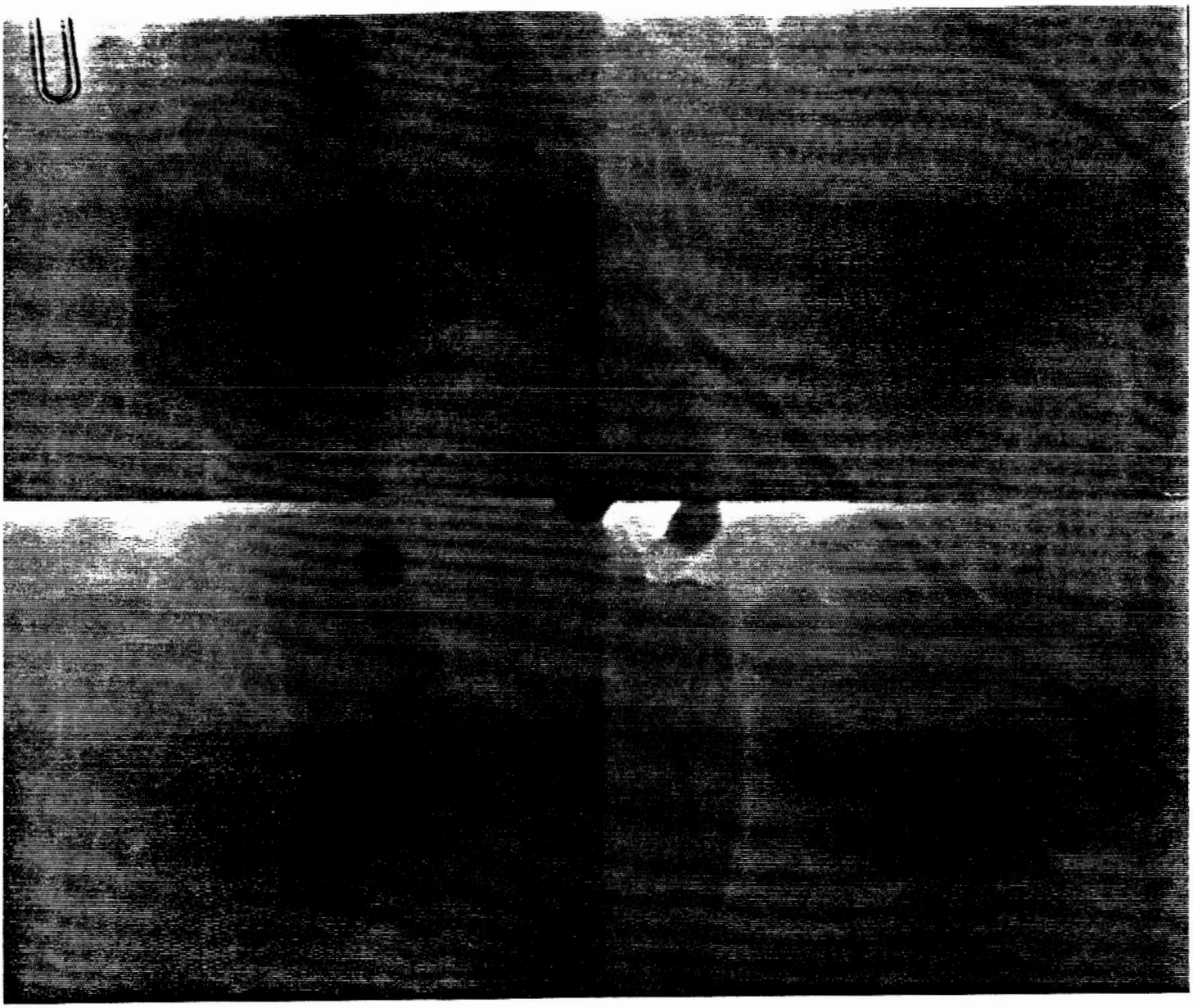

Figure 4. Estimation of d(x,y)

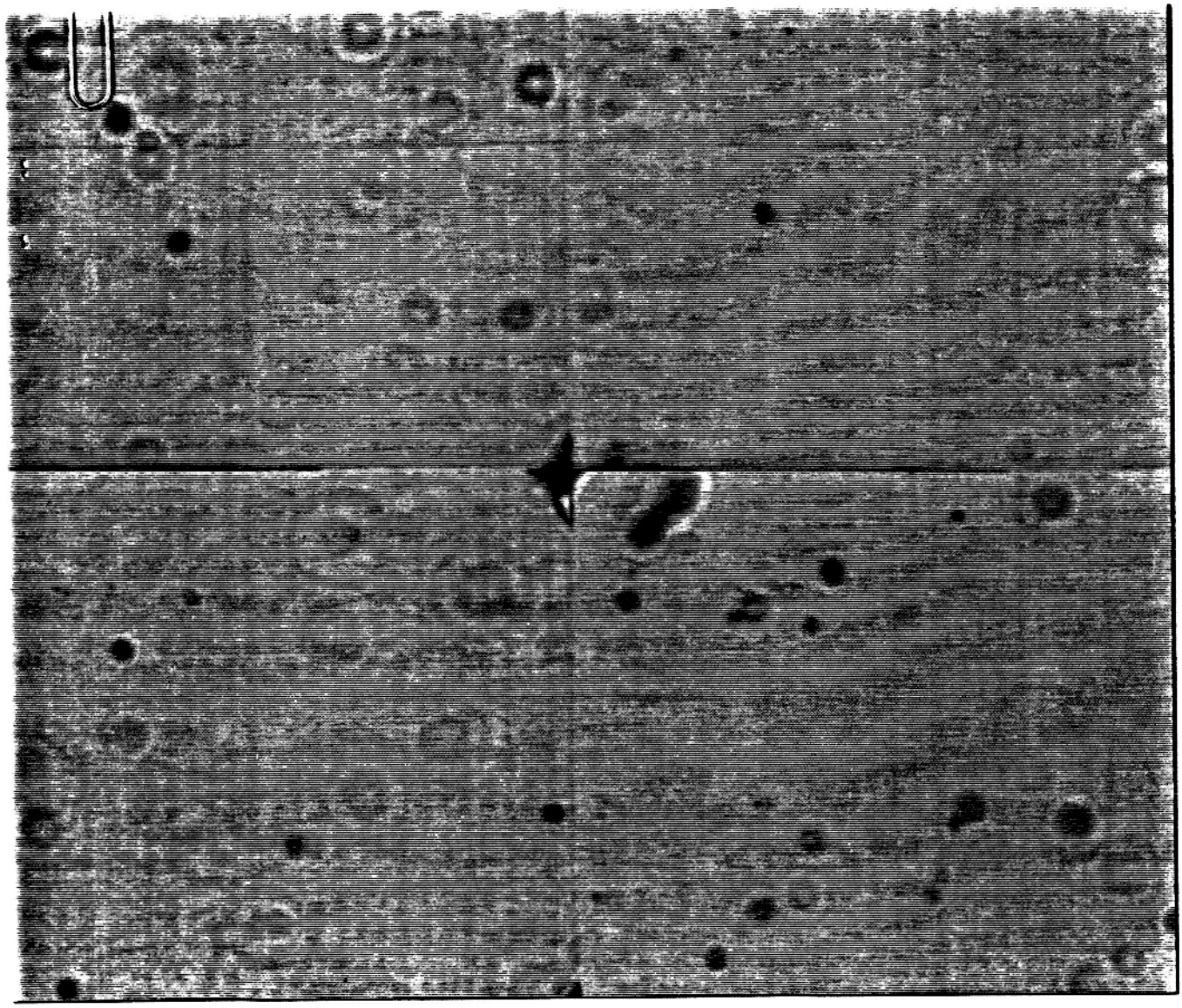

Figure 5. Normalized image

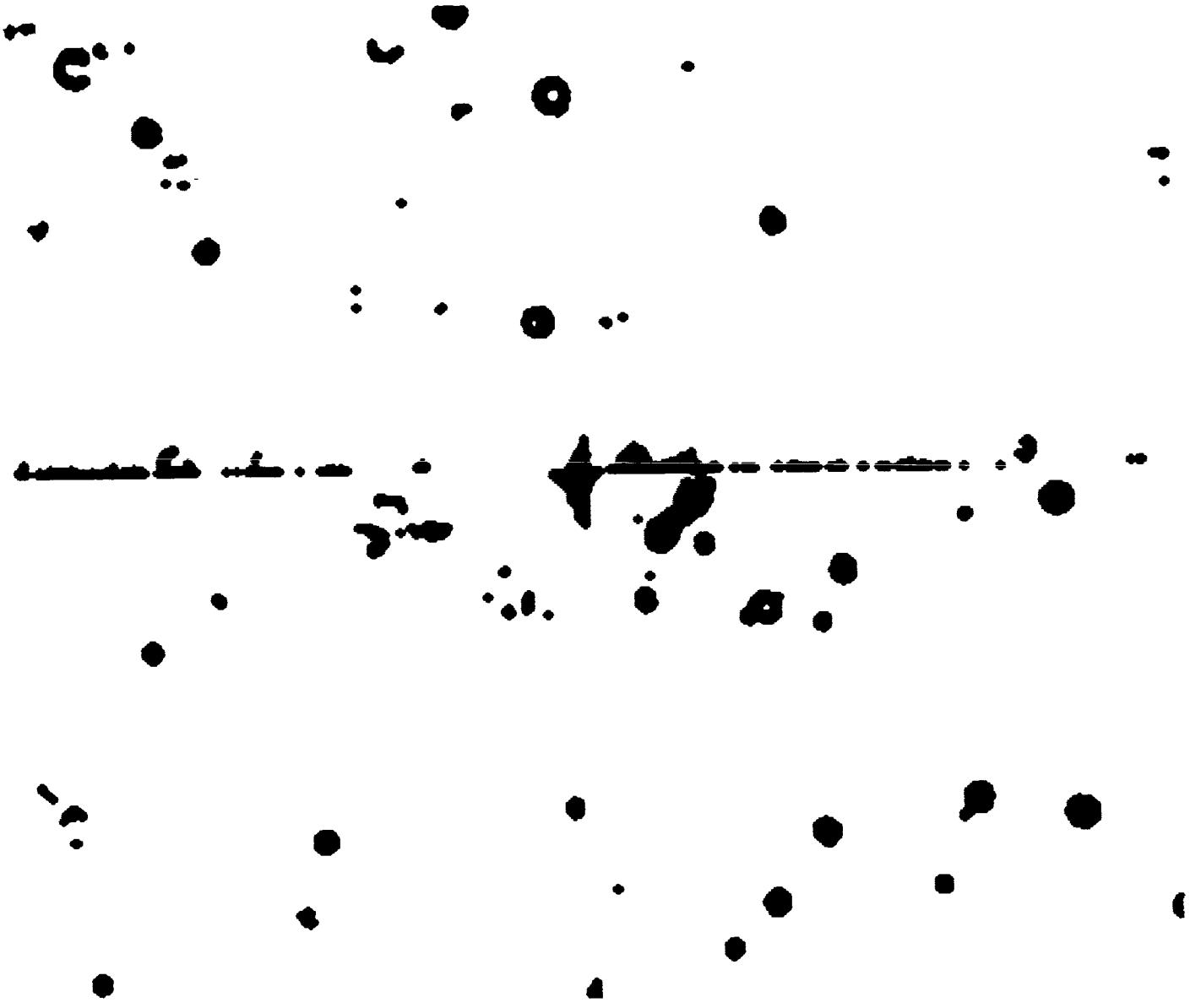

Figure 6. Threshold image

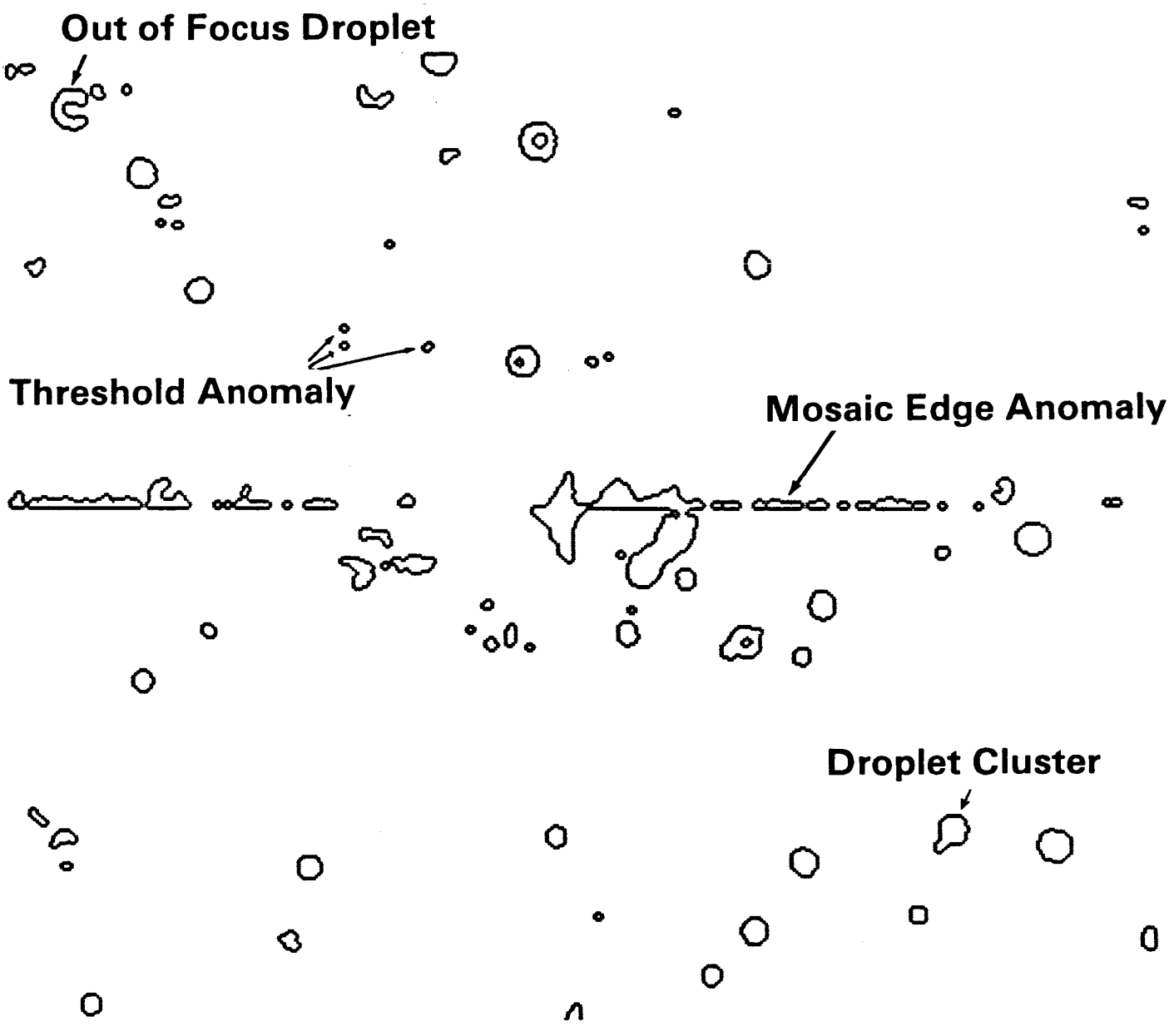

Figure 7. Boundary image

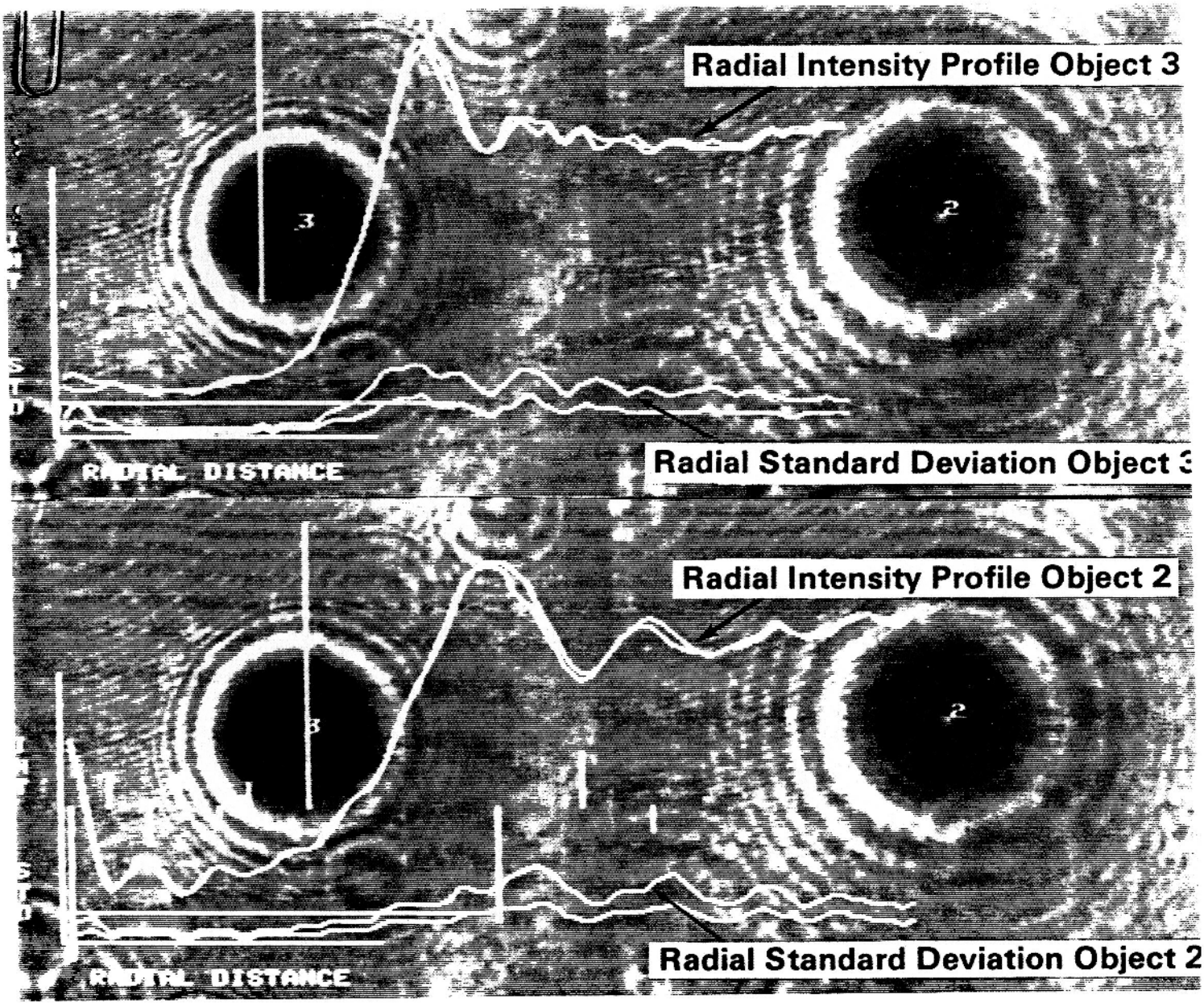

Figure 8. Radial and Standard deviation curve for candidate

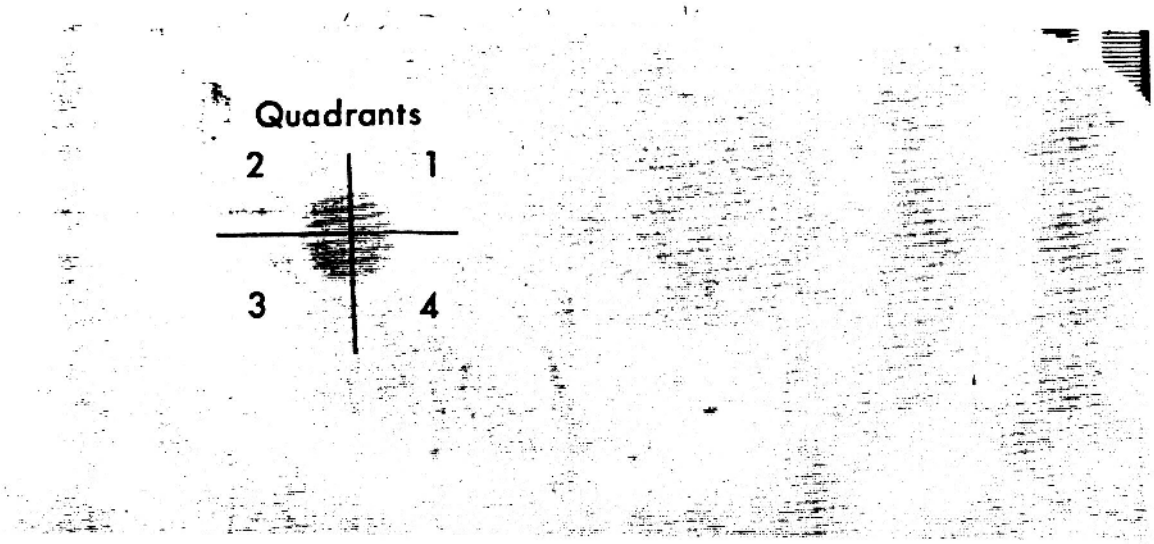

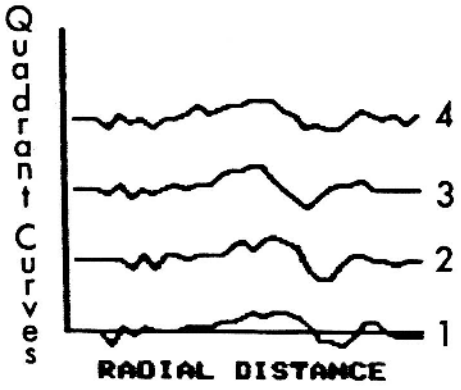

Before reposition

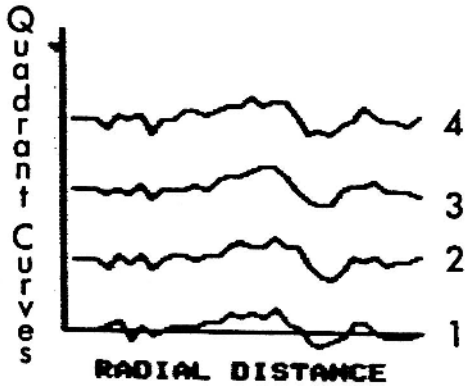

After reposition

Figure 9. Quadrant plots for deviation derivatives

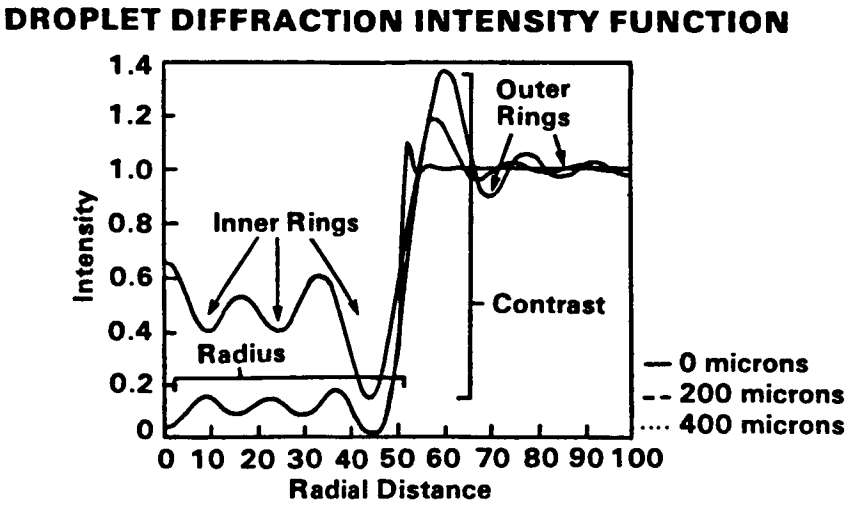

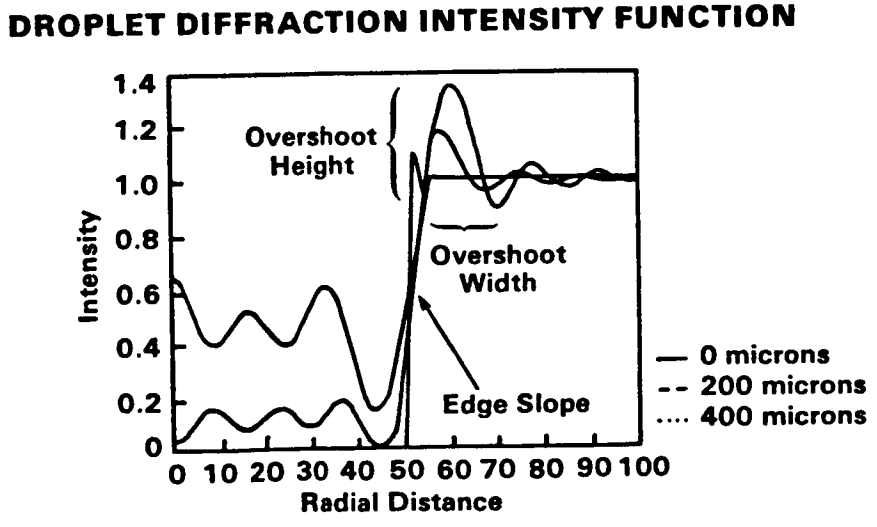

Figure 10. Feature measurement

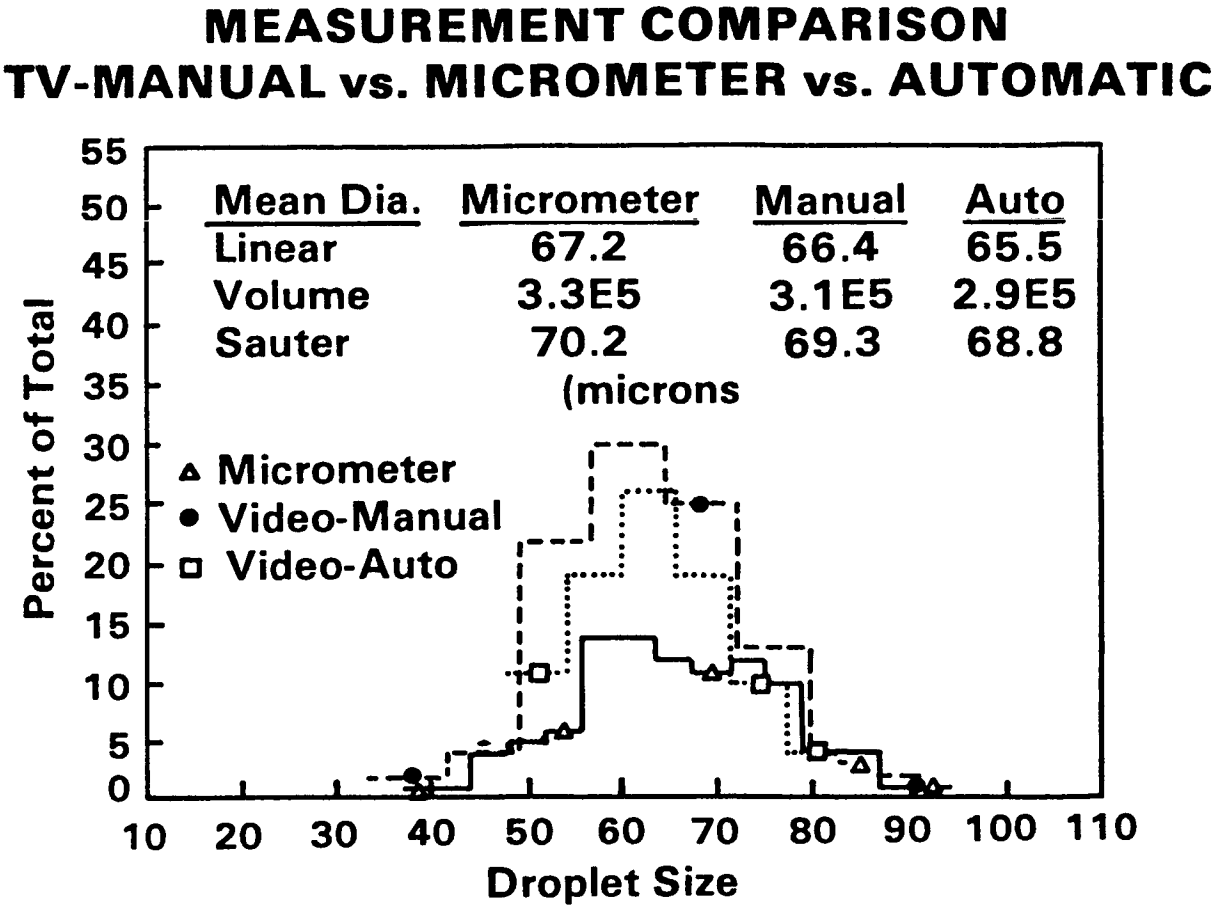

Figure 11. Synthesized distribution on microscope slide

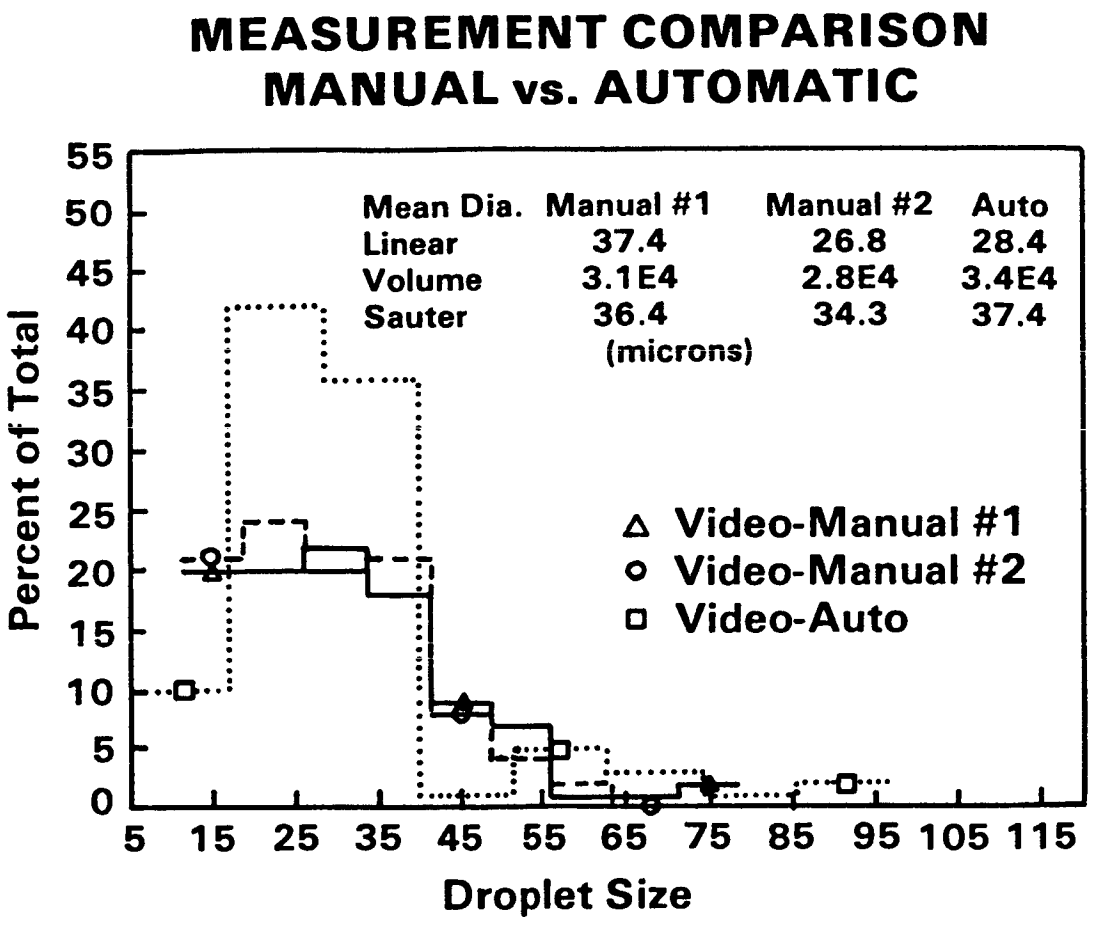

Figure 12. Heptane spray

Figure Legend

1. Equipment block diagram
2. Gaussian filtering operation
3. Original Image
4. Estimation of d(x,y)
5. Normalized image
6. Threshold image
7. Boundary image
8. Radial and Standard deviation curve for candidate
9. Quadrant plots for deviation derivatives
10. Feature measurement
11. Synthesized distribution on microscope slide
12. Heptane spray